Richha Sharma[1], Vikash Ghlawat[2], Zoran Radaković[3], Khursheed Alam[2]*

CREEP STRESS ANALYSIS OF FUNCTIONALLY GRADED TRANSVERSELY ISOTROPIC PIEZOELECTRIC DISC WITH VARIABLE THICKNESS UNDER ROTATION

ANALIZA NAPONA PUZANJA FUNKCIONALNOG KOMPOZITNOG TRANSVERZALNO IZOTROPNOG PIJEZOELEKTRIČNOG ROTIRAJUĆEG DISKA PROMENLJIVE DEBLJINE

Originalni naučni rad / Original scientific paper
Rad primljen / Paper received: 6.06.2024

Adresa autora / Author's address:
[1] Department of Mathematics, Jaypee Institute of Information Technology, Noida, India 0009-0007-2895-9626
[2] Dept. of Mathematics, SBSR, Sharda University, Gr. Noida, India, *email: vikashgahlawat25@gmail.com
[3] University of Belgrade, Faculty of Mechanical Engineering, Belgrade, Serbia 0000-0001-8054-470X

Keywords
- functionally graded
- piezoelectric
- rotating disc
- transversely isotropic
- creep

Abstract

Materials exhibiting different piezoelectric properties throughout their volume are referred to as functionally graded piezoelectric materials (FGPM). Due to their graded composition, the characteristics of these materials can be customized to fit particular needs in a variety of applications. Functionally graded piezoelectric materials are beneficial in many technical applications because of their versatility that enables increased performance, efficiency, and adaptability in a variety of disciplines. The objective of the current study is to analyse creep stresses in an annular disc composed of transversely isotropic, functionally graded piezoelectric material with varying thickness parameters. Creep stresses are evaluated analytically using the approach of Seth's transition theory. By using the stress-strain relations, the equations for mechanical stresses and electrical displacement are determined. Substituting these relations into the equilibrium equation a nonlinear differential equation is obtained. The findings are presented both numerically and graphically, demonstrating how the thickness parameter affects the circumferential stresses in the intermediate surface of the rotating disc. The disc made of transversely isotropic piezoelectric material PZT-4 exhibits higher creep stresses than other materials under consideration according to all of the numerical discussions and calculations. This work may provide an effective methodology for the analysis of functionally graded piezoelectric rotating discs and contribute to theoretical research and engineering applications.

Ključne reči
- funkcionalni kompozitni materijal
- pijezoelektrični
- rotirajući disk
- transverzalno izotropni
- puzanje

Izvod

Materijali koji pokazuju različite pijezoelektrične osobine u svojoj zapremini tretiraju se kao funkcionalni kompozitni pijezoelektrični materijali (FGPM). Usled njihovog kompozitnog sastava, karakteristike ovih materijala se mogu menjati prema specifičnim potrebama u raznim primenama. Funkcionalni kompozitni pijezoelektrični materijali imaju prednosti u mnogim primenama u tehnici zbog njihove svestranosti koja omogućava poboljšanje performansi, efikasnost i adaptabilnost u raznim disciplinama. Cilj rada je analiza napona puzanja u prstenastom disku sačinjenog od transverzalno izotropnog, funkcionalnog kompozitnog pijezoelektričnog materijala sa parametrima promenljive debljine. Naponi puzanja se određuju analitički, primenom pristupa teorije prelaznih napona Seta. Korišćenjem izraza napona-deformacija određuju se jednačine mehaničkih napona i električnih pomeranja. Smenom ovih izraza u jednačinu ravnoteže dobija se nelinearna diferencijalna jednačina. Rezultati su predstavljeni numerički i grafički kako bi se uočio uticaj parametar debljine na obimske napone u međuslojevima rotirajućeg diska. Disk sačinjen od transverzalnog izotropnog pijezoelektričnog materijala PZT-4 pokazuje veće napone puzanja u odnosu na ostale razmatrane materijale, shodno svim diskusijama numerike i proračuna. Ovaj rad pruža delotvornu metodologiju u analizi funkcionalnog kompozitnog pijezoelektričnog rotirajućeg diska i doprinosi teorijskom istraživanju i inženjerskim primenama.

INTRODUCTION

Functionally graded materials can be designed using either a macro- or microscale method. In the macroscale technique, a functionally graded piezoelectric material occupies the place of the standard piezoelectric active element. Consequently, depending on a particular gradation function, all or some of the properties (piezoelectric, dielectric, or elastic properties) vary along a specified direction, usually throughout its thickness. A dielectric substance that permits an immediate interaction between electrical and elastic energy is called a piezoelectric material. A piezoelectric material undergoes dimensional changes in the presence of an electric field and, in turn, produces a dielectric displacement in response to mechanical stress. Quartz, tourmaline, and Rochelle salt are among the materials that naturally exhibit the piezoelectric effect. Other polycrystalline materials that can be subjected to this phenomenon include barium titanate ($BaTiO_3$), polyvinylidene fluoride (PVDF), and lead zirconate titanate (PZT4). A specific kind of moderate mechanical deformation known as creep deformation happens when a material is subjected to high stress levels over an extended length of time. The comparatively slow rate of creep deformation might lead to a material failing below its yield point.

Numerous researchers examine the elastic, plastic, and creep deformations in different solid structures. Betton /1/ employed mathematical concepts to determine the creep stress performance in thick-walled shells under inner surface pressure. Through the use of an identical elastic approach, Penny /2/ ascertained the effects of creep in the cylinder. Creep deformation in a revolving disc composed of transversely isotropic material with variable density shaft under heat gradient is evaluated by Temesgen et al. /3/. After studying thermal stresses in thick-walled circular cylinders under both internal and external pressure, Sharma et al. /4/ came to the conclusion that thicker circular cylinders with less compressible walls that experience thermal effects under both internal and external pressure and have nonlinear measures are preferable. After analysing the creep stresses in a transversely isotropic circular cylinder under inner surface pressure, Sharma et al. /5/ conclude that a non-homogeneous cylinder is a superior option. Dynamic problem in piezo-electric microstretch thermoelastic material under laser heat source was studied by Kumar and Ailwalia /6/. The creep stresses in a thin rotating disc made of piezoelectric material are analysed by Sharma and Sahni /7/, who found that the stresses greatly increase with pressure and angular velocity. After creep stress analysis in rotating discs, Sharma et al. /8/ came to the conclusion that extremely non-homogeneous disks are a better alternative for designing purposes than homogeneous disks. Two-dimensional deformations in a rotating, nonhomogeneous, isotropic, magneto-thermoelastic medium were examined by Gunghas et al. /9/. The deformation in a two-dimensional functionally graded thermoelastic micro-elongated medium was examined by Kalkal et al. /10/. Saadatfar et al. /11/ evaluated the deformation and stress of a functionally graded piezoelectric rotating disc that was subjected to mechanical and thermomechanical loads, including heat transfer via radiation and convection. The results show that the convection boundary, the thickness function, the inhomogeneity index, and solar radiation all have a major impact on the responses of the spinning FGPM disc. In an annular isotropic disc under internal pressure, Chand et al. /12/ investigated the stresses and found that, for compressible material, hoop stress is maximal near the disc's outer surface, in contrast to incompressible material. Es-Saheb and Fouad /13/ examined the creep behaviour of a rotating thick-walled Al-SiC_p composite cylinder under constant load and pressure from the outside and inside using the finite element approach. They found that as the internal pressure in the cylinder increases, so do the strain rates. Using optical microscopy and mechanical stress testing, Matvienko et al. /14/ investigated the plastic deformation of a rotating annular disc composed of alloys hardened by dispersion to aluminium. By applying mid-zone theory to analyse the stresses in a thin annular transversely isotropic piezoelectric disc with varying thickness and density, Sharma /15/ discovered that a piezoelectric disc composed of barium titanate $BaTiO_3$ outperforms a piezoceramic disc constructed of PZT4. An analytical technique was used by Sharma and Nagar /16/ to assess the stresses in a functionally graded piezoelectric disc with variable compressibility and variable density. They discovered that an annular disc composed of PZT-4 is superior for engineering designs. The nonlinear dynamics of functionally graded porous annular plates under different time-dependent loads was studied by Jafary and Taghizadeh /17/. These findings provide insightful information that can be used to improve plate design and performance. Daghigh et al. /18/ conducted a time-dependent creep investigation of functionally graded spinning discs with varying thickness at extremely high temperatures. The significance of taking creep effects into account when designing FGM rotating discs is highlighted by their research. Saadatfar et al. /19/ study the thermoelastic creep evolution in a variable thickness functionally graded piezoelectric rotating annular plate taking radiation and convection heat transport into consideration. Godana et al. /20/ determined the stress distribution throughout the shell surface by applying Seth's mid-zone concept to generalize strain measure theory for the modelling of elastoplastic deformation in a transversely isotropic shell under a temperature gradient and constant pressure.

In this paper, creep stresses are computed in a functionally graded transversely isotropic piezoelectric rotating disc under the influence of pressure on inner and outer surfaces. The transversely isotropic features of creep material and the piezo-electric effect have been taken into consideration in this study. Concept of Seth's transition theory is applied to rotating discs in order to evaluate creep stresses. The resulting quantities are depicted graphically to explore the effect of piezoelectric parameters and internal pressure.

MATHEMATICAL FORMULATION

A rotating disc with internal and external radii a and b, respectively, and angular velocity denoted by ω subjected to internal pressure (p_1) and external pressure (p_2) is considered. The choice of a thin disc is made to focus on the state of plane stress, specifically, $T_{zz} = 0$.

Displacement components are

$$u = r(1-\beta)\,,\; v = 0\,,\; w = dz\,,\; \beta = f(r)\,, \qquad (1)$$

where: β is a function of $r = \sqrt{(x^2 + y^2)}$ and d is a constant.

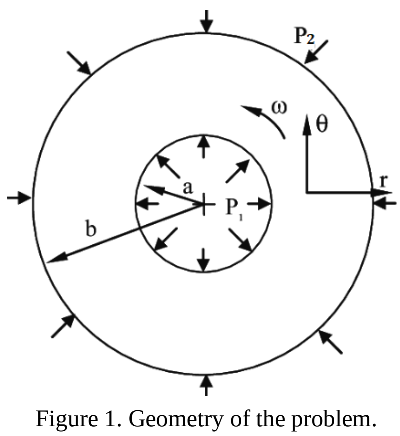

Figure 1. Geometry of the problem.

Stress-strain relations for this problem are as follows

$$t_{rr}=c_{11}e_{rr}+(c_{11}-2c_{66})e_{\theta\theta}+c_{13}e_{zz}-e_{11}E_r\,,$$
$$t_{\theta\theta}=(c_{11}-2c_{66})e_{rr}+c_{11}e_{\theta\theta}+c_{13}e_{zz}-e_{12}E_r\,,$$
$$t_{zz}=t_{zr}=t_{r\theta}=t_{\theta z}=0\,. \qquad (2)$$

Components of strain are as follows:

$$e_{rr}=\frac{1}{n}[1-(r\beta'+\beta)^n]=\frac{1}{n}[1-\beta^n(1+p)^n]\,,$$
$$e_{\theta\theta}=\frac{1}{n}[1-\beta^n]\,,\; e_{zz}=\frac{1}{n}[1-(1-d)^n]\,,$$
$$E_r=\frac{1}{\eta_{11}}\left[\frac{1}{r}-\frac{e_{11}}{n}(1-\beta^n(1+\rho)^n)-\frac{e_{12}}{n}(1-\beta^n)\right], \qquad (3)$$

functionally graded,

$$c_{11}=c_{011}\left(\frac{r}{b}\right)^k,\; c_{66}=c_{066}\left(\frac{r}{b}\right)^k,\; c_{13}=c_{013}\left(\frac{r}{b}\right)^k,$$
$$c_{12}=c_{012}\left(\frac{r}{b}\right)^k,\; h=h_0\left(\frac{r}{b}\right)^m. \qquad (4)$$

Equation of equilibrium for rotating disc:

$$\frac{d}{dr}(hrT_{rr})-hT_{\theta\theta}+\rho h\omega^2r^2=0\,. \qquad (5)$$

Putting the values from Eq.(2) in Eq.(5), we obtain

$$\frac{d}{dr}\left\{h_0\left(\frac{r}{b}\right)^m r(c_{11}e_{rr}+(c_{11}-2c_{66})e_{\theta\theta}+c_{13}e_{zz}-e_{11}E_r)\right\}-h_0\left(\frac{r}{b}\right)^m\{(c_{11}-2c_{66})e_{rr}+c_{11}e_{\theta\theta}+c_{13}e_{zz}-e_{12}E_r\}+\rho h_0\left(\frac{r}{b}\right)^m\omega^2r^2=0\,.$$

Using Eq.(4) in the previous equation, we have

$$\frac{d}{dr}\left\{h_0\left(\frac{r}{b}\right)^m r\left\{c_{011}\left(\frac{r}{b}\right)^k e_{rr}+(c_{011}\left(\frac{r}{b}\right)^k-2c_{066}\left(\frac{r}{b}\right)^k\right\}e_{\theta\theta}+c_{013}\left(\frac{r}{b}\right)^k e_{zz}-e_{11}E_r\right\}-h_0\left(\frac{r}{b}\right)^m\left\{\left\{c_{011}\left(\frac{r}{b}\right)^k-2c_{066}\left(\frac{r}{b}\right)^k\right\}e_{rr}+\right.$$
$$\left.+c_{011}\left(\frac{r}{b}\right)^k e_{\theta\theta}+c_{013}\left(\frac{r}{b}\right)^k e_{zz}-e_{12}E_r\right\}+\rho h_0\left(\frac{r}{b}\right)^m\omega^2r^2=0\,.$$

Firstly, we find

$$\frac{d}{dr}(hrT_{rr})=\frac{d}{dr}[hr\{c_{11}e_{rr}(c_{11}-2c_{66})e_{\theta\theta}+c_{13}e_{zz}-e_{11}E_r\}]=\frac{d}{dr}\left\{rh_0\left(\frac{r}{b}\right)^m c_{011}\left(\frac{r}{b}\right)^k\frac{1}{n}[1-\beta^n(1+p)^n]+rh_0\left(\frac{r}{b}\right)^m(c_{011}-2c_{066})\times\right.$$
$$\left.\times\left(\frac{r}{b}\right)^k\frac{1}{n}(1-\beta^n)+rh_0\left(\frac{r}{b}\right)^m c_{013}\left(\frac{r}{b}\right)^k\frac{1}{n}[1-(1-d)^n]-rh_0\left(\frac{r}{b}\right)^m e_{11}\frac{1}{\eta_{11}}\left[\frac{1}{r}-\beta^n(1+p)^n\right]+\frac{r}{\eta_{11}}h_0\left(\frac{r}{b}\right)^m\frac{e_{12}}{n}e_{11}(1-\beta^n)\right\}$$
$$=(r\beta'+\beta)^{n-1}\frac{d}{dr}(r\beta'+\beta)\left\{-\frac{h_0c_{011}}{n}n\left(\frac{1}{b}\right)^{k+m}r^{k+m+1}-\frac{nh_0e_{11}^2}{n\eta_{11}b^m}r^{m+1}\right\}+\beta^{n-1}\frac{d\beta}{dr}\left\{-n\frac{n_0c_{011}}{nb^{k+m}}r^{k+m+1}+\frac{2nh_0c_{066}}{nb^{k+m}}r^{k+m+1}-\frac{nh_0e_{11}e_{12}}{n\eta_{11}b^m}r^m\right\}+$$
$$+(1-\beta^n)\left\{\frac{h_0c_{011}}{nb^{k+m}}(k+m+1)r^{k+m}-\frac{2h_0c_{066}}{nb^{k+m}}(k+m+1)r^{k+m}+\frac{h_0e_{11}e_{12}m}{n\eta_{11}b^m}r^{m-1}\right\}+(1-(r\beta'+\beta)^n)\left\{\frac{h_0c_{011}}{nb^{k+m)}}(k+m+1)r^{k+m}+\frac{h_0e_{11}^2}{n\eta_{11}b^m}(m+1)r^m\right\}+$$
$$+\frac{h_0c_{013}}{nb^{k+m}}(k+m+1)(1-(1-d)^n)r^{k+m}-\frac{h_0e_{11}}{\eta_{11}b^m}mr^{m-1}, \qquad (6)$$

$$T_{\theta\theta}=\left\{h_0\left(\frac{r}{b}\right)^m\left[\left\{c_{011}\left(\frac{r}{b}\right)^k-2c_{066}\left(\frac{r}{b}\right)^k\right\}\frac{1}{n}(1-(r\beta'+\beta)^n)+c_{013}\left(\frac{r}{b}\right)^k\frac{1}{n}(1-(1-d)^n)+c_{011}\left(\frac{r}{b}\right)^k\frac{1}{n}(1-\beta^n)-\right.\right.$$
$$\left.\left.-e_{12}\frac{1}{\eta_{11}}\left\{\frac{1}{r}-\frac{e_{11}}{n}(1-(r\beta'+\beta)^n\right\}+\frac{e_{12}^2}{n\eta_{11}}(1-\beta^n)\right.\,. \qquad (7)$$

Putting the value of $\frac{d}{dr}(hrT_{rr})$ and $T_{\theta\theta}$ in Eq.(5), we have

$$r(r\beta'+\beta)^{n-1}\frac{d}{dr}(r\beta'+\beta)\left\{-h_0c_{011}\left(\frac{r}{b}\right)^{k+m}-\frac{h_0e_{11}^2}{\eta_{11}}\left(\frac{r}{b}\right)^m\right\}+r\beta^{n-1}\frac{d\beta}{dr}\left\{-h_0c_{011}\left(\frac{r}{b}\right)^{k+m}+2h_0c_{066}\left(\frac{r}{b}\right)^{k+m}-\frac{h_0e_{11}e_{12}}{\eta_{11}}\frac{1}{r}\left(\frac{r}{b}\right)^m\right\}+$$
$$+\frac{1}{n}(1-\beta^n)\left\{h_0c_{011}(k+m+1)\left(\frac{r}{b}\right)^{k+m}-2h_0c_{066}(k+m+1)\left(\frac{r}{b}\right)^{k+m}+mh_0e_{11}e_{12}\frac{1}{r}\left(\frac{r}{b}\right)^m-h_0c_{011}\left(\frac{r}{b}\right)^{k+m}-\frac{h_0e_{12}^2}{\eta_{11}}\left(\frac{r}{b}\right)^m\right\}+$$
$$+\frac{1}{n}(1-(r\beta'+\beta)^n)\left\{h_0c_{011}(k+m+1)\left(\frac{r}{b}\right)^{k+m}+\frac{h_0e_{11}^2}{\eta_{11}}(m+1)\left(\frac{r}{b}\right)^m-h_0c_{011}\left(\frac{r}{b}\right)^{k+m}+2h_0c_{066}\left(\frac{r}{b}\right)^{k+m}-\frac{e_{11}e_{12}}{\eta_{11}}\left(\frac{r}{b}\right)^m\right\}+$$
$$+\frac{1}{n}(1-(1-d)^n)\left\{h_0c_{013}(k+m+1)\left(\frac{r}{b}\right)^{k+m}-h_0c_{013}\left(\frac{r}{b}\right)^{k+m}\right\}-\frac{h_0e_{11}}{\eta_{11}}\frac{m}{r}\left(\frac{r}{b}\right)^m+\frac{h_0e_{12}}{\eta_{11}}\frac{1}{r}\left(\frac{r}{b}\right)^m+\rho h_0\left(\frac{r}{b}\right)^m\omega^2r^2=0\,, \qquad (8)$$

where, $r\beta'=\beta P$.

So, the equations are

$$r(r\beta'+\beta)^{n-1}\frac{d}{dr}(r\beta'+\beta)=\beta^n p(1+p)^n+\beta^{n+1}p(1+p)^{n-1}\frac{dp}{d\beta}\,, \qquad (9)$$

$$\frac{1}{n}[1-(r\beta'+\beta)^n]=\frac{1}{n}[1-\beta^n(1+p)^n]\,, \qquad (10)$$

$$r\beta^{n-1}\frac{d\beta}{dr}=\beta^n p\,. \qquad (11)$$

By utilizing Eqs.(9)-(11) in Eq.(7), we obtain:

$$\Big\{\beta^n(1+p)^n+\beta^{n+1}p(1+p)^{n-1}\frac{dp}{d\beta}\Big\}\Big\{-h_0c_{011}\left(\frac{r}{b}\right)^{k+m}-\frac{h_0e_{11}^2}{\eta_{11}}\left(\frac{r}{b}\right)^m\Big\}+\beta^n p\Big\{-h_0c_{011}\left(\frac{r}{b}\right)^{k+m}+2h_0c_{066}\left(\frac{r}{b}\right)^{k+m}-\frac{h_0e_{11}e_{12}}{\eta_{11}}\frac{1}{r}\left(\frac{r}{b}\right)^m\Big\}+$$
$$+\frac{1}{n}(1-\beta^n)\Big\{h_0(k+m+1)(c_{011}-2c_{066})\left(\frac{r}{b}\right)^{k+m}+mh_0e_{11}e_{12}\frac{1}{r}\left(\frac{r}{b}\right)^m-h_0c_{011}\left(\frac{r}{b}\right)^{k+m}-\frac{h_0e_{12}^2}{\eta_{11}}\left(\frac{r}{b}\right)^m\Big\}+\frac{1}{n}[1-\beta^n(1+p)^n]\times$$
$$\times\Big\{h_0c_{011}(k+m)\left(\frac{r}{b}\right)^{k+m}+\frac{h_0e_{11}^2}{\eta_{11}}\left(\frac{r}{b}\right)^m+2h_0c_{066}\left(\frac{r}{b}\right)^{k+m}-\frac{e_{11}e_{12}}{\eta_{11}}\left(\frac{r}{b}\right)^m\Big\}+\frac{1}{n}(1-(1-d)^n)\Big\{h_0c_{013}(k+m)\left(\frac{r}{b}\right)^{k+m}\Big\}-\frac{h_0e_{11}}{\eta_{11}}\frac{m}{r}\left(\frac{r}{b}\right)^m+$$
$$+\frac{h_0e_{12}}{\eta_{11}}\frac{1}{r}\left(\frac{r}{b}\right)^m+\rho h_0\omega^2r^2\left(\frac{r}{b}\right)^m=0,$$

$$-\Big\{c_{011}\beta^{n+1}+\beta^{n+1}\left(\frac{r}{b}\right)^{-k}\frac{e_{11}^2}{\eta_{11}}\Big\}p(1+p)^{n-1}\frac{dp}{d\beta}=+\beta^n p\Big\{c_{011}-2c_{066})\left(\frac{r}{b}\right)^k-\frac{e_{11}e_{12}}{\eta_{11}}\frac{1}{r}\Big\}-\frac{1}{n}(1-\beta^n)\Big\{(k+m+1)(c_{011}-2c_{066})\left(\frac{r}{b}\right)^k+$$
$$+\frac{m}{r}e_{11}e_{12}-c_{011}\left(\frac{r}{b}\right)^k-\frac{e_{12}^2}{\eta_{11}}\Big\}-\frac{1}{n}[1-\beta(1+p)^n]\Big\{(k+m)c_{011}\left(\frac{r}{b}\right)^k+\frac{e_{11}^2}{\eta_{11}}(k+1)+2c_{066}\left(\frac{r}{b}\right)^k-\frac{e_{11}e_{12}}{\eta_{11}}\Big\}-\frac{1}{n}(1-(1-d)^n)\times$$
$$\times\Big\{c_{013}(k+m)\left(\frac{r}{b}\right)^k\Big\}+m\frac{e_{11}}{\eta_{11}}\frac{1}{r}-\frac{e_{12}}{\eta_{11}}\frac{1}{r}-\rho\omega^2r^2. \tag{12}$$

Boundary conditions are assumed

$$T_{rr}=-p_1 \quad \text{at} \quad r=a; \quad T_{rr}=-p_2 \quad \text{at} \quad r=b. \tag{13}$$

CONVERSION OF ELASTIC STATE INTO CREEP STATE

Transition theory states that at a critical point $P\to-1$, a material changes from an elastic to a creep state. For evaluation of stresses, transition function R is assumed as

$$R=T_{rr}-T_{\theta\theta},$$

$$R=\Big\{c_{011}\left(\frac{r}{b}\right)^k\frac{1}{n}[1-\beta^n(1+p)^n]+(c_{011}-2c_{066})\left(\frac{r}{b}\right)^k\frac{1}{n}(1-\beta^n)+c_{013}\left(\frac{r}{b}\right)^k\frac{1}{n}(1-(1-d)^n)-\frac{e_{11}}{\eta_{11}}\left(\frac{1}{r}\right)+\frac{e_{11}^2}{n\eta_{11}}[1-\beta^n(1+p)^n]+\frac{e_{11}e_{12}}{\eta_{11}n}(1-\beta^n)\Big\}-$$
$$-\Big\{(c_{011}-2c_{066})\left(\frac{r}{b}\right)^k\frac{1}{n}[1-\beta^n(1+p)^n]+c_{011}\left(\frac{r}{b}\right)^k\frac{1}{n}(1-\beta^n)+c_{013}\left(\frac{r}{b}\right)^k\frac{1}{n}(1-(1-d)^n)-\frac{e_{11}}{\eta_{11}}\left(\frac{1}{r}\right)+\frac{e_{11}e_{12}}{n\eta_{11}}[1-\beta^n(1+p)^n]+\frac{e_{12}^2}{\eta_{11}n}(1-\beta^n)\Big\} \tag{14}$$

Taking logarithmic differentiation of Eq.(14), we get

$$\frac{d}{dr}(\log R)=\frac{d}{dr}\log[T_{rr}-T_{\theta\theta}]=\frac{1}{T_{rr}-T_{\theta\theta}}\frac{d}{dr}[T_{rr}-T_{\theta\theta}].$$

Now we find first, $\frac{d}{dr}[T_{rr}-T_{\theta\theta}]$,

$$\frac{d}{dr}[T_{rr}-T_{\theta\theta}]=\frac{1}{n}\frac{d}{dr}\Big\{(1-(r\beta'+\beta)^n)\Big[2c_{066}\left(\frac{r}{b}\right)^k+\frac{e_{11}^2}{\eta_{11}}-\frac{e_{11}e_{12}}{\eta_{11}}\Big]+(1-\beta^n)\Big[-2c_{066}\left(\frac{r}{b}\right)^k-\frac{e_{12}^2}{\eta_{11}}+\frac{e_{11}e_{12}}{\eta_{11}}\Big]\Big\}=\frac{1}{n}\Big\{-n\Big[(r\beta'+\beta)^{n-1}\frac{d}{dr}(r\beta'+\beta)\Big]\times$$
$$\times\Big[2c_{066}\left(\frac{r}{b}\right)^k+\frac{e_{11}^2}{\eta_{11}}-\frac{e_{11}e_{12}}{\eta_{11}}\Big]+(1-(r\beta'+\beta)^n)\Big\{2c_{066}\frac{k}{r}\left(\frac{r}{b}\right)^k\Big\}-n\beta^{n-1}\frac{d\beta}{dr}\Big[-2c_{066}\left(\frac{r}{b}\right)^k-\frac{e_{12}^2}{\eta_{11}}+\frac{e_{11}e_{12}}{\eta_{11}}\Big]-(1-\beta^n)\Big\{2c_{066}\frac{k}{r}\left(\frac{r}{b}\right)^k\Big\}\Big\} \tag{15}$$

$$\frac{1}{T_{rr}-T_{\theta\theta}}\frac{d}{dr}[T_{rr}-T_{\theta\theta}]=\frac{1}{n}\frac{-n\Big\{(r\beta'+\beta)^{n-1}\frac{d}{dr}(r\beta'+\beta)\Big\}\Big\{2c_{066}\left(\frac{r}{b}\right)^k+\frac{e_{11}^2}{\eta_{11}}-\frac{e_{11}e_{12}}{\eta_{11}}\Big\}+(1-(r\beta'+\beta)^n)\Big\{2c_{066}\frac{k}{r}\left(\frac{r}{b}\right)^k\Big\}-}{[(1-(r\beta'+\beta)^n]\Big\{2c_{066}\left(\frac{r}{b}\right)^k+\frac{e_{11}^2}{\eta_{11}}-\frac{e_{11}e_{12}}{\eta_{11}}\Big\}+(1-\beta^n)\times}$$
$$\frac{-n\beta^{n-1}\frac{d\beta}{dr}\Big\{-2c_{066}\left(\frac{r}{b}\right)^k-\frac{e_{12}^2}{\eta_{11}}+\frac{e_{11}e_{12}}{\eta_{11}}\Big\}-(1-\beta^n)\Big\{2c_{066}\frac{k}{r}\left(\frac{r}{b}\right)^k\Big\}}{\times\Big\{-2c_{066}\left(\frac{r}{b}\right)^k-\frac{e_{12}^2}{\eta_{11}}+\frac{e_{11}e_{12}}{\eta_{11}}\Big\}}, \tag{16}$$

$$\frac{d}{dr}(\log R)=\frac{2c_{066}\left(\frac{r}{b}\right)^k\frac{k}{r}+\frac{n}{r}\beta^n\Big\{-2c_{066}\left(\frac{r}{b}\right)^k-\frac{e_{12}^2}{\eta_{11}}+\frac{e_{11}e_{12}}{\eta_{11}}\Big\}-2c_{066}\left(\frac{r}{b}\right)^k\frac{k}{r}(1-\beta^n)}{2c_{066}\left(\frac{r}{b}\right)^k+\frac{e_{11}^2}{\eta_{11}}-\frac{e_{11}e_{12}}{\eta_{11}}+(1-\beta^n)\Big\{-2c_{066}\left(\frac{r}{b}\right)^k\Big\}}. \tag{17}$$

Taking the value of $\beta=D/r$ as $P\to-1$, and D is constant,

$$\frac{d}{dr}(\log R)=\frac{2c_{066}\left(\frac{r}{b}\right)^k\frac{k}{r}+\frac{n}{r}\left(\frac{D}{r}\right)^n\left\{-2c_{066}\left(\frac{r}{b}\right)^k-\frac{e_{12}^2}{\eta_{11}}+\frac{e_{11}e_{12}}{\eta_{11}}\right\}-2c_{066}\left(\frac{r}{b}\right)^k\frac{k}{r}\left[1-\left(\frac{D}{r}\right)^n\right]}{2c_{066}\left(\frac{r}{b}\right)^k+\frac{e_{11}^2}{\eta_{11}}-\frac{e_{11}e_{12}}{\eta_{11}}+\left[1-\left(\frac{D}{r}\right)^n\right]\left\{-2c_{066}\left(\frac{r}{b}\right)^k\right\}},$$

$$\frac{d}{dr}\log R=G\rightarrow\log R=\int Gdr+\log A,\qquad R=Ae^{\int Gdr}=AH, \tag{18}$$

where: $H=e^{\int Gdr}$; and
$$G=\frac{2c_{066}\left(\frac{r}{b}\right)^k\frac{k}{r}+\frac{n}{r}\left(\frac{D}{r}\right)^n\left\{-2c_{066}\left(\frac{r}{b}\right)^k-\frac{e_{12}^2}{\eta_{11}}+\frac{e_{11}e_{12}}{\eta_{11}}\right\}-2c_{066}\left(\frac{r}{b}\right)^k\frac{k}{r}\left[1-\left(\frac{D}{r}\right)^n\right]}{2c_{066}\left(\frac{r}{b}\right)^k+\frac{e_{11}^2}{\eta_{11}}-\frac{e_{11}e_{12}}{\eta_{11}}+\left[1-\left(\frac{D}{r}\right)^n\right]\left\{-2c_{066}\left(\frac{r}{b}\right)^k-\frac{e_{12}^2}{\eta_{11}}+\frac{e_{11}e_{12}}{\eta_{11}}\right\}}.$$

Boundary conditions are as

$$t_{rr}=-p_1 \text{ at } r=a \text{ and } t_{rr}=-p_2 \text{ at } r=b. \tag{19}$$

As the equation of equilibrium is given by

$$\frac{d}{dr}(t_{rr})-\frac{t_{rr}-t_{\theta\theta}}{r}+\rho\omega^2 r=0. \tag{20}$$

Putting the value from Eq.(18) in Eq.(20) and integrating

$$t_{rr}=\int\frac{AH}{r}dr-\frac{\rho\omega^2 r^2}{2}+B. \tag{21}$$

From Eq.(14) and Eq.(18) we have

$$t_{\theta\theta}=\int\frac{AH}{r}dr-\frac{\rho\omega^2 r^2}{2}-AH+B. \tag{22}$$

Applying boundary condition $t_{rr} = -p_1$ at $r = a$, we get

$$\left[A\int\frac{H}{r}dr\right]_{r=a}-\frac{\rho\omega^2 a^2}{2}+B=-p_1. \tag{23}$$

Applying boundary condition $t_{rr} = -p_2$ at $r = b$, we get

$$\left[A\int\frac{H}{r}dr\right]_{r=b}-\frac{\rho\omega^2 b^2}{2}+B=-p_2. \tag{24}$$

Using Eq.(21) and Eq.(22), we obtain

$$p_1-p_2+\frac{\rho\omega^2(a^2-b^2)}{2}=A\left\{\left[\int\frac{H}{r}dr\right]_{r=b}-\left[\int\frac{H}{r}dr\right]_{r=a}\right\}.$$

Now we have found the values of A and B,

$$A=\frac{p+\frac{\rho\omega^2(a^2-b^2)}{2}}{\int_a^b\frac{H}{r}dr}, \tag{25}$$

$$B=\frac{\rho\omega^2 b^2}{2}-\frac{p+\frac{\rho\omega^2(a^2-b^2)}{2}}{\int_a^b\frac{H}{r}dr}\left[\int\frac{H}{r}dr\right]_{r=b}, \tag{26}$$

where: $p = p_1 - p_2$.

Now, the non-dimensional form of all the parameters is defined as

$$R=\frac{r}{b},\ R_0=\frac{a}{b},\ \sigma_r=\frac{t_{rr}}{p},\ \sigma_\theta=\frac{t_{\theta\theta}}{p},\ \Omega=\frac{\rho\omega^2 b^2}{p}. \tag{27}$$

Stresses in non-dimension form are as follows:

$$\sigma_r=\frac{t_{rr}}{p}=\frac{2p+\Omega(R_0^2-1)}{2\int_{R_0}^1\frac{H_1}{R}dR}\int\frac{H_1}{R}dR-\frac{\Omega}{2R^2}+$$
$$+\Omega-\frac{2p+\Omega(R_0^2-1)}{2\int_{R_0}^1\frac{H_1}{R}dR}\left[\int\frac{H}{R}dR\right]_{R=1},$$

$$\sigma_\theta=\frac{t_{\theta\theta}}{p}=\frac{2p+\Omega(R_0^2-1)}{2\int_{R_0}^1\frac{H_1}{R}dR}\left(\int\frac{H_1}{R}dR-H_1\right)-\frac{\Omega}{2R^2}+$$
$$+\Omega-\frac{2p+\Omega(R_0^2-1)}{2\int_{R_0}^1\frac{H_1}{R}dR}\left[\int\frac{H}{R}dR\right]_{R=1}, \tag{28}$$

where: $H_1=e^{\int G_1 dr}$; and
$$G_1=\frac{2c_{066}(R)^k\frac{k}{Rb}+\frac{n}{Rb}\left(\frac{D}{Rb}\right)^n\left\{-2c_{066}(R)^k-\frac{e_{12}^2}{\eta_{11}}+\frac{e_{11}e_{12}}{\eta_{11}}\right\}-2c_{066}(R)^k\frac{k}{Rb}\left[1-\left(\frac{D}{Rb}\right)^n\right]}{2c_{066}(R)^k+\frac{e_{11}^2}{\eta_{11}}-\frac{e_{11}e_{12}}{\eta_{11}}+\left[1-\left(\frac{D}{Rb}\right)^n\right]\left\{-2c_{066}(R)^k-\frac{e_{12}^2}{\eta_{11}}+\frac{e_{11}e_{12}}{\eta_{11}}\right\}}.$$

NUMERICAL DISCUSSIONS

Figures 2 to 9 depict creep stresses for linear measure (n = 1 and 2) and angular velocities (Ω = 50 and 100) with varying radii ratios $R = r/b$ for functionally graded transversely isotropic (magnesium) and functionally graded transversely isotropic piezoelectric (PZT4 and $BaTiO_3$) materials. Figures 2a and 2b depict creep stresses for measures n = 1 and 2 with angular velocities Ω = 50 and 100 and pressure p = 5, k = 1. From Fig. 2a it is observed that creep stresses are compressive at the inner surface of the disc and tensile at the outer surface. For all the materials being considered for linear measure, these creep stresses rise with increasing radii ratio and reach their maximal value at the outer surface of the disc, also the stresses are maximum for functionally graded transversely isotropic piezoelectric material $BaTiO_3$. From Fig. 2b it is observed that the stresses increase with increasing angular velocity. With increasing value of pressure (p = 10), the stresses increase significantly as noticed from Fig. 3. Figures 4 and 5 represent creep stresses for linear measure n = 1 with angular velocities Ω = 50 and 100 and pressure p = 5 and 10, and k = 2. Tensile stresses are observed at the disc's outer surface, and they are highest for transversely isotropic FG material like magnesium. Also, the stresses increase with increase in angular velocity and pressure.

Creep stresses for nonlinear measure $n = 2$ with angular velocity $\Omega = 50$ and 100 and pressure $p = 5$ and 10, and $k = 1$ are shown in Figs. 5 and 6. It is observed in Fig. 6 that creep stresses are tensile and possess maximum value for transversely isotropic piezoelectric FG material PZT4 as compared to other materials. Figure 7 illustrates how stress values significantly increase as pressure and angular velocity increase. Creep stresses for nonlinear measure $n = 2$ with angular velocity $\Omega = 50$ and 100 and pressure $p = 5$ and 10, and $k = 2$, are shown in Figs. 8 and 9. The stresses are compressive at the inner surface for materials PZT4 and Mg, and tensile at the outer surface. These stresses are maximum for piezoelectric $BaTiO_3$. Figure 8 demonstrates that when pressure and angular velocity rise, the stresses rise noticeably.

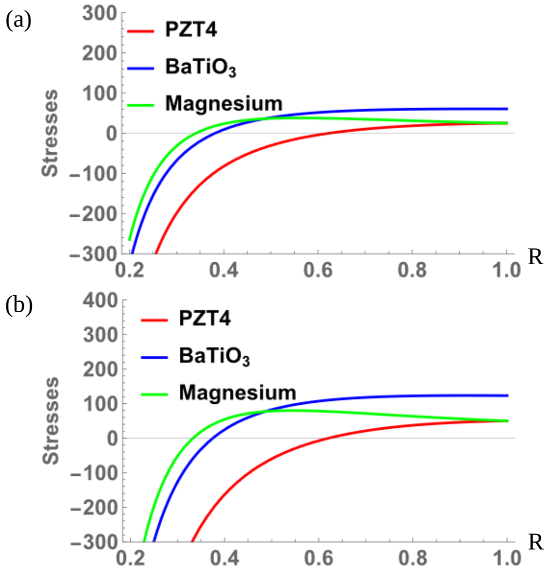

Figure 2. Graphs of creep stresses with angular velocity $\Omega = 50$ and 100, $p = 5$, $k = 1$ and $n = 1$.

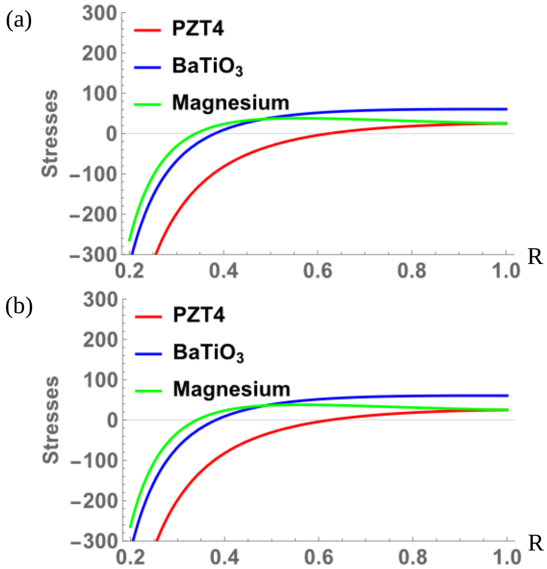

Figure 3. Graphs of creep stresses with angular velocity $\Omega = 50$ and 100, $p = 5$, $k = 1$, and $n = 1$.

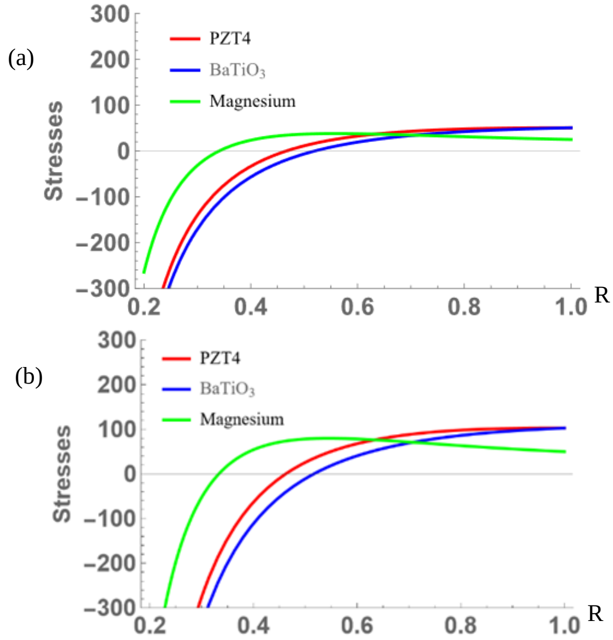

Figure 4. Graphs of creep stresses with angular velocity $\Omega = 50$ and 100, $p = 5$, $k = 2$, and $n = 1$.

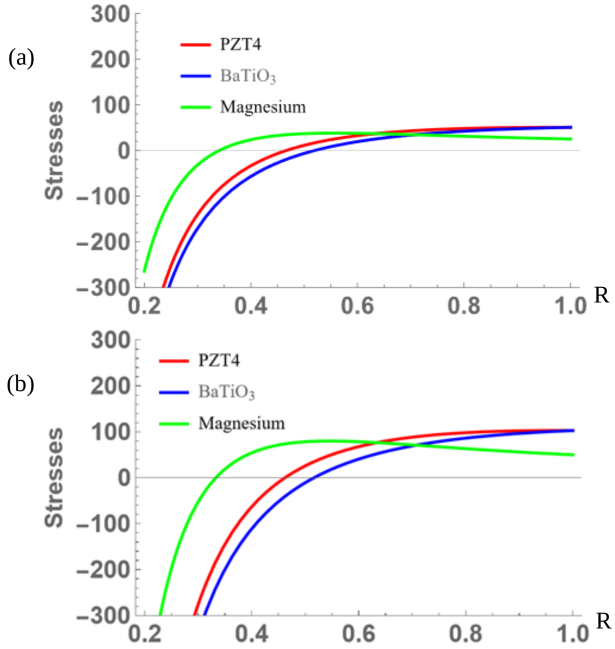

Figure 5. Graphs of creep stresses with angular velocity $\Omega = 50$ and 100, $p = 10$, $k = 2$, and $n = 1$.

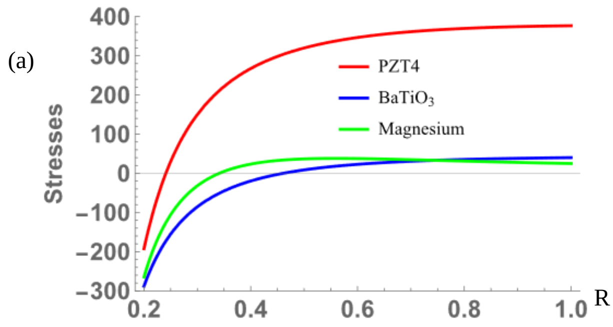

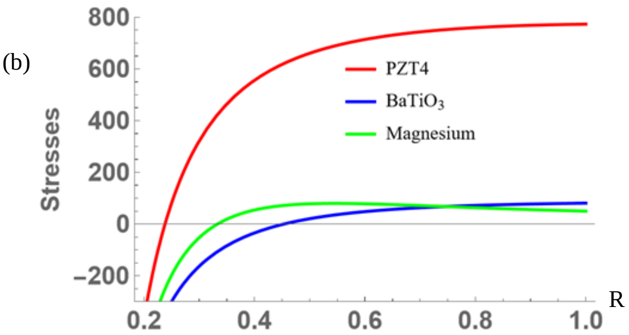

Figure 6. Graphs of creep stresses with angular velocity Ω = 50 and 100, p = 5, k = 1, and n =2.

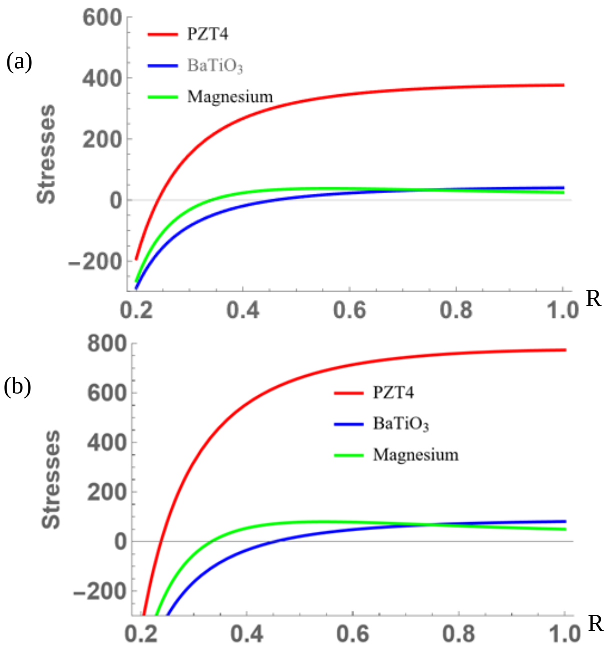

Figure 7. Graphs of creep stresses with angular velocity Ω = 50 and 100, p = 10, k = 1, and n =2.

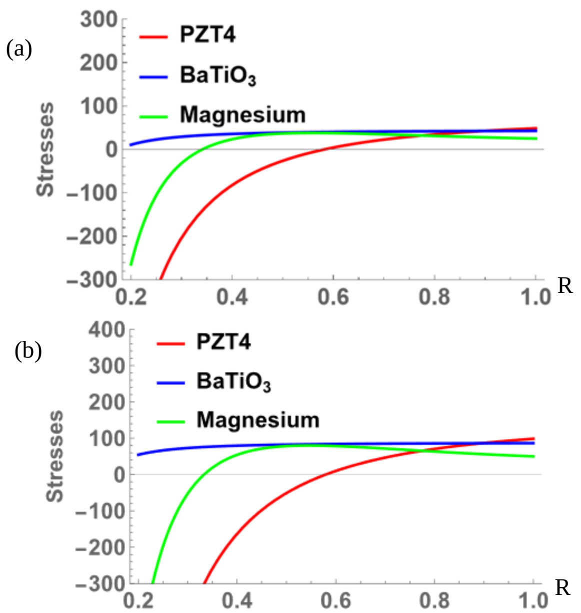

Figure 8. Graphs of creep stresses with angular velocity Ω = 50 and 100, p = 5, k = 2, and n =2.

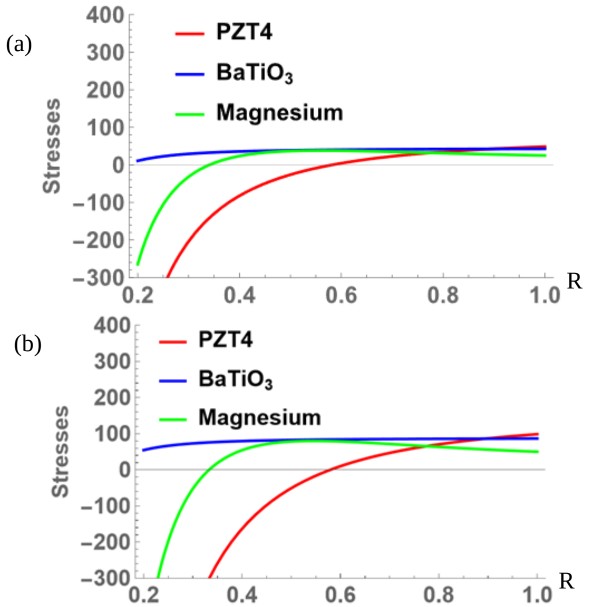

Figure 9. Graphs of creep stresses with angular velocity Ω = 50 and 100, p = 10, k =2, and n =2.

CONCLUSION

The creep stresses and the piezo-electric effect in a transversely isotropic functionally graded rotating disc are examined. The problem is solved using an analytical approach. Numerical solutions for the creep stress components have been obtained. To investigate the impact of the piezoelectric parameter, the obtained quantities are visually represented. Based on all the graphs and numerical calculations, it is found that the disc made of transversely isotropic piezoelectric material PZT-4 demonstrates higher creep stresses than other materials under investigation, as based on all the graphs and numerical calculations. This work may provide an effective methodology for the analysis of functionally graded piezoelectric rotating discs and contribute to the theoretical research and engineering applications.

REFERENCES

1. Betten, J., Creep Mechanics, 2nd Ed., Springer, Berlin, 2005.
2. Penny, R.K., Marriott, D.L., Design for Creep, 2nd Ed., McGraw Hill, Springer, 1995.
3. Temesgen, A.G., Singh, S.B., Pankaj, T. (2020), *Modeling of creep deformation of a transversely isotropic rotating disc with a shaft having variable density and subjected to a thermal gradient*, Therm. Sci. Eng. Prog. 20: 100745. doi: 10.1016/j.tsep.2020.100745
4. Sharma R., Sharma S., Radaković, Z. (2018), *Thermal creep analysis of pressurized thick-walled circular cylindrical vessels*, Struct. Integr. Life, 18(1): 7-14.
5. Sharma, S., Sharma, R., Panchal, R. (2018), *Creep transition in transversely isotropic composite circular cylinder subjected to internal pressure*, Int. J Pure Appl. Math. 120(1): 87-96. doi: 10.12732/ijpam.v120i1.8
6. Kumar, A., Ailawalia, P. (2019), *Dynamic problem in piezoelectric microstretch thermoelastic medium under laser heat source*, Multidisc. Model. Mater. Struct. 15(2): 473-491. doi: 10.1108/MMMS-04-2018-0077
7. Sharma, R., Sahni, M. (2020), *Analysis of creep stresses in thin rotating disc composed of piezoelectric material*, Struct. Integr. Life, Special Issue 2020: S45-S49.

8. Sharma, S., Sahni, M., Sharma, R. (2017), *Creep deformation of a non-homogeneous thin rotating disk of exponentially varying thickness with internal pressure*, AIP Conf. Proc. 1897(1): 020 011. doi: 10.1063/1.5008690
9. Gunghas, A., Kumar, R., Deswal, S., Kalkal, K.K. (2019), *Influence of rotation and magnetic fields on a functionally graded thermoelastic solid subjected to a mechanical load*, J Math. 2019: 1016981. doi: 10.1155/2019/1016981
10. Kalkal, K.K., Gunghas, A., Deswal, S. (2020), *Two-dimensional magneto-thermoelastic interactions in a micropolar functionally graded solid*, Mech. Based Des. Struct. Mach. 48(3): 348-369. doi: 10.1080/15397734.2019.1652100
11. Saadatfar, M., Babazadeh, M.A., Babaelahi, M. (2024), *Stress and deformation of a functionally graded piezoelectric rotating disk with variable thickness subjected to magneto-thermo-mechanical loads including convection and radiation heat transfer*, Int. J Appl. Mech. 16(01): 2450002. doi: 10.1142/S175882512 4500029
12. Chand, S., Sood, S., Thakur, P., Gupta, K. (2023), *Elasto-plastic stress deformation in an annular disk made of isotropic material and subjected to uniform pressure*, Struct. Integr. Life, 23(1): 61-64.
13. Es-Saheb, M.H., Fouad, Y. (2023), *Creep analysis of rotating thick cylinders subjected to external and internal pressure: Analytical and numerical approach*, Appl. Sci. 13(21): 11652. doi: 10.3390/app132111652
14. Matvienko, O., Daneyko, O., Valikhov, V., et al. (2023), *Elasto-plastic deformation of rotating disk made of aluminum dispersion-hardened alloys*, Metals, 13(6): 1028. doi: 10.3390/met13 061028
15. Sharma, R. (2023), *Evaluation of thermal elastic-plastic stresses in transversely isotropic disk made of piezoelectric material with variable thickness and variable density subjected to internal pressure*, Struct. Integr. Life, 23(2): 205-212.
16. Sharma, R., Nagar, A. (2024), *Analytical approach on stress analysis in a functionally graded piezoelectric annular disk with varying compressibility and varying density under internal pressure*, Int. J Non-Linear Mech. 162(6): 104723. doi: 10.1016/j.ij nonlinmec.2024.104723
17. Jafary, H., Taghizadeh, M. (2023), *Nonlinear dynamics response of porous functionally graded annular plates using modified higher order shear deformation theory*, SN Appl. Sci. 5: 368. doi: 10.1007/s42452-023-05591-6
18. Daghigh, V., Edalati, H., Daghigh, H., et al. (2023), *Time-dependent creep analysis of ultra-high-temperature functionally graded rotating disks of variable thickness*, Forces in Mech. 13: 100235. doi: 10.1016/j.finmec.2023.100235
19. Saadatfar, M., Babazadeh, M.A., Babaelahi, M. (2024), *Thermo-elastic creep evolution in a variable thickness functionally graded piezoelectric rotating annular plate considering convection and radiation heat transfer*, Mech. Based Des. Struct. Machines, 53 (8): 5944-5969. doi: 10.1080/15397734.2023.2266826
20. Godana., T.A., Singh, S.B., Thakur, P., Kumar, P. (2023), *Modelling the elastoplastic deformation of an internally pressurized transversely isotropic shell under a temperature gradient*, Turk. J Comp. Math. Educ. (TURCOMAT), 14(1): 207-221. doi: 10. 17762/turcomat.v14i1.13458